Nanoprobe diffusion in entangled polymer solutions: Linear vs. unconcatenated ring chains

Negar Nahali, and Angelo Rosa

Citation: The Journal of Chemical Physics **148**, 194902 (2018); doi: 10.1063/1.5022446
View online: https://doi.org/10.1063/1.5022446
View Table of Contents: http://aip.scitation.org/toc/jcp/148/19
Published by the American Institute of Physics

Nanoprobe diffusion in entangled polymer solutions: Linear vs. unconcatenated ring chains

Negar Nahali[a] and Angelo Rosa[b]
Sissa (Scuola Internazionale Superiore di Studi Avanzati), Via Bonomea 265, 34136 Trieste, Italy

(Received 15 January 2018; accepted 1 May 2018; published online 17 May 2018)

We employ large-scale molecular dynamics computer simulations to study the problem of nanoprobe diffusion in entangled solutions of linear polymers and unknotted and unconcatenated circular (ring) polymers. By tuning both the diameter of the nanoprobe and the density of the solution, we show that nanoprobes of diameter smaller than the entanglement distance (tube diameter) of the solution display the same (Rouse-like) behavior in solutions of both polymer architectures. Instead, nanoprobes with larger diameters appear to diffuse markedly faster in solutions of rings than in solutions of linear chains. Finally, by analysing the distribution functions of spatial displacements, we find that nanoprobe motion in rings' solutions shows both Gaussian and ergodic behaviors, in all regimes considered, while, in solutions of linear chains, nanoprobes exceeding the size of the tube diameter show a transition to non-Gaussian and non-ergodic motion. Our results emphasize the role of chain architecture in the motion of nanoprobes dispersed in polymer solutions. *Published by AIP Publishing.*
https://doi.org/10.1063/1.5022446

I. INTRODUCTION

The micro-mechanical and viscoelastic properties of complex polymer fluids and, more in general, of soft and biological materials can be efficiently explored owing to the advent of *microrheology*,[1–8] a versatile technique based on the direct tracking of the diffusive motion of nanoprobes injected into the medium. Through the analysis of the motion of the probes, one can measure the mechanical response of the material and get quantitative information about its elastic and viscous properties typically on larger time and length scales and at higher resolution than by traditional rheology. At the same time, given amounts of nanoprobes embedded in polymer matrices may be employed to alter significantly their mechanical properties and thus contribute to the design of novel materials.[9,10]

The study of nanoprobe motion in semi-dilute and concentrated solutions (melts) of polymer chains constitutes an important and yet largely unexplored chapter in the long history of microrheology.[9,11–18] These systems appear in fact particularly challenging due to the complex interplay between different length scales such as nanoprobe size, mesh size of the polymer solution, and chain contour length.

More recently, it has been suggested[15,17,18] that another factor, namely, *chain architecture*, may play a quite subtle role when it comes to describe the detailed motion of nanoprobes. In particular, by considering the two examples of entangled solutions of linear chains *vs.* unknotted and unconcatenated circular (ring) chains, Nahali and Rosa[15] and Ge *et al.*[17] have shown that nanoprobes of linear sizes *larger* than the mesh size of the solution move definitely *faster* in solutions of rings than in solutions of linear chains. In the same paper, Ge *et al.* described a theory where the observed discrepancy is understood in terms of the different spatial and temporal behaviors of linear chains *vs.* rings in solution.

Under the same environmental conditions, linear chains and rings in solution do behave in fact quite differently: in particular, because the unconcatenation constraint rings fold into self-similar, compact conformations with non-Gaussian statistics and because the lack of free ends do not perform reptation,[19–46] both features being instead well established trademarks of linear chains in solution.[47–49] Moreover, the presence of threadings between close-by ring polymers in high density solutions has been held responsible for chain dynamics becoming glassy and heterogenous,[44,46] a feature, once again, completely absent in linear chains. All these features are likely to influence the motion of nanoprobes embedded in the solution.

Motivated by these considerations, in this paper, we (re)consider the problem of nanoprobe motion in entangled solutions of linear *vs.* ring polymers. By employing large scale Molecular Dynamics (MD) computer simulations, we provide a quantitative, in-depth description of nanoprobe dynamics in terms of chain architecture and topological constraints between close-by chains. Mainly, the present work extends the numerical analysis pioneered by Refs. 15 and 17 along two directions: (1) we consider wider ranges for probe sizes and solution densities and (2) we provide a systematic characterization of nanoprobe dynamics in terms of the (van-Hove) probability distribution function of spatial displacements and other observables borrowed from the theory of glassy systems[50] which allow us to define the conditions under which nanoprobe dynamics shifts from Gaussian/ergodic to non-Gaussian/non-ergodic behavior.

[a]Electronic mail: nenahali@sissa.it
[b]Electronic mail: anrosa@sissa.it

The paper is structured as follows: In Sec. II, we give a concise account of the state-of-the-art concerning single-chain conformations and nanoprobe diffusion in entangled solutions of linear chains and rings. In Sec. III, we explain the computational model and the numerical methods employed in the article. In Sec. IV, we describe in detail our results and interpret some of them in the light of the theoretical framework of Sec. II. Finally, in Sec. V, we summarize the main conclusions with an outlook for future work.

II. THEORY

In this section, we describe (Sec. II A) the relevant physics of polymer conformations in entangled solutions and we highlight, in particular, the main differences between linear chains and rings. This is followed (Secs. II B and II C) by a concise account of the scaling theory by Ge *et al.*[12,14,17] linking chain statistics to nanoprobe diffusion.

A. Polymer conformations in entangled solutions: Linear *vs.* ring chains

The physics of polymer conformations in entangled solutions can be described in terms of a set of few relevant length scales:[47–49] (1) The microscopic correlation length, ξ, defined as the average spatial distance from a monomer on one chain to the nearest monomer on another chain. (2) The Kuhn length of the polymer fiber, ℓ_K, characterizing the crossover from rigid rod to random coil behavior. (3) The entanglement length, L_e, corresponding to the chain contour length spanning the tube-like region where topological constraints from surrounding polymers confine each given chain. The length scale $d_T \approx \sqrt{L_e \ell_K}$ corresponds to the *tube diameter* (see Sec. III D), which is a measure for the mesh size of the solution.

On chain contour lengths $L \lesssim L_e$, topological constraints play no role and linear and ring chains display the same behavior, the mean-square end-to-end distances characterized by the familiar crossover from rigid rod to random coil behavior at ℓ_K

$$\langle R^2(L)\rangle_{\text{lin, ring}} \approx \begin{cases} L^2, & L \lesssim \ell_K \\ \ell_K L, & \ell_K \lesssim L \lesssim L_e \end{cases}. \tag{1}$$

On larger contour lengths $L \gtrsim L_e$, linear chains remain ideal because of the screening of excluded volume effects,[47–49] while the additional unlinking constraint forces rings into space-filling compact conformations.[26,27,31,32] Summarizing

$$\langle R^2(L)\rangle_{\text{lin}} \approx \ell_K L_e \left(\frac{L}{L_e}\right)^1, \tag{2}$$

$$\langle R^2(L)\rangle_{\text{ring}} \approx \ell_K L_e \left(\frac{L}{L_e}\right)^{2/3}. \tag{3}$$

B. Nanoprobe motion: Solutions of linear polymers

The erratic motion of a single nanoprobe can be captured[51] by its mean-square displacement (MSD), $\Delta r^2(\mathcal{T};\tau)$, as a function of the lag-time τ and the measurement time $\mathcal{T}$

$$\Delta r^2(\mathcal{T};\tau) \equiv \frac{1}{\mathcal{T}-\tau}\int_0^{\mathcal{T}-\tau} (\vec{r}(t+\tau)-\vec{r}(t))^2 dt, \tag{4}$$

where $\vec{r}(t)$ is the nanoprobe spatial position at time t. The time-average displacement can be defined as

$$\Delta r^2(\tau) \equiv \lim_{\mathcal{T}\to\infty} \Delta r^2(\mathcal{T};\tau), \tag{5}$$

while its ensemble average is defined as

$$\langle \Delta r^2(\mathcal{T};\tau)\rangle \equiv \frac{1}{N_{\text{np}}}\sum_{i=1}^{N_{\text{np}}} \Delta r_i^2(\mathcal{T};\tau) \tag{6}$$

with the sum indicating that the average is performed over the whole set of N_{np} independent nanoprobes used to explore the system. Accordingly, we indicate the time- *and* ensemble-average displacement as $\langle \Delta r^2(\tau)\rangle$.

According to nanoprobe diameter d, three regimes can be distinguished:

(I) Small nanoprobes, $d \lesssim \xi$. In this case, nanoprobe motion is barely influenced by the surrounding polymers and its MSD is described by

$$\langle \Delta r^2(\tau)\rangle_{\text{lin}} \approx D_s\,\tau \approx \frac{\kappa_B T}{\eta_s\, d}\,\tau, \tag{7}$$

where D_s is the diffusion coefficient, η_s is the viscosity of the solvent, κ_B is the Boltzmann constant, and T is the temperature.

(II) Intermediate nanoprobes, $\xi \lesssim d \lesssim d_T$. Now, nanoprobe motion is affected by the polymers and its MSD displays three regimes

$$\langle \Delta r^2(\tau)\rangle_{\text{lin}} \approx \begin{cases} D_s\,\tau, & \tau < \tau_\xi \approx \frac{\eta_s \xi^3}{\kappa_B T}, \quad \text{(a)} \\ D_s \tau_\xi \left(\frac{\tau}{\tau_\xi}\right)^{1/2}, & \tau_\xi < \tau < \tau_d \approx \tau_\xi \left(\frac{d}{\xi}\right)^4, \quad \text{(b)} \\ D_s \left(\frac{\xi}{d}\right)^2 \tau, & \tau > \tau_d. \quad \text{(c)} \end{cases} \tag{8}$$

At short times [Eq. (8a)], nanoprobe motion is driven only by random collisions with the solvent, as in I. This regime stops at τ_ξ, the relaxation time of a polymer strand of spatial size ξ. Then [Eq. (8b)], the nanoprobe experiences a time-dependent viscosity $\eta(\tau) \approx \eta_s\, n_{str}(\tau) \equiv \eta_s \left(\frac{\tau}{\tau_\xi}\right)^{1/2}$, where $n_{str}(\tau)$ is the number of strands which have relaxed at time τ. This regime stops at time τ_d, the relaxation time of a larger polymer strand of spatial size = $d = \xi\sqrt{n_{str}(\tau_d)}$. Above τ_d [Eq. (8c)], nanoprobe motion becomes diffusive again with effective viscosity $\approx \eta_s \cdot n_{str}(\tau_d)$, which is $\approx (d/\xi)^2$ times *larger* than the value in pure solvent.

(III) Large nanoprobes, $d \gtrsim d_T$. The regime described by Eq. (8a) still holds, while the regime of Eq. (8b) stops at $\tau_{d=d_T} = \tau_\xi \left(\frac{d_T}{\xi}\right)^4$. Above τ_{d_T}, nanoprobes are *trapped* by entanglements and the MSD becomes plateau-like: $\langle \Delta r^2(\tau)\rangle_{\text{lin}} = \langle \Delta r^2(\tau_{d_T})\rangle_{\text{lin}} \approx D_s \left(\frac{\xi}{d_T}\right)^2 \tau_{d_T} \approx \frac{\xi}{d} d_T^2$. Interestingly, this last expression depends on all three relevant time scales of the problem. Neglecting hopping[14] between close-by entanglements, the trapping regime persists up to complete chain reptation[48] at $\tau \approx \tau_{\text{rep}} \approx \tau_e \left(\frac{L_c}{L_e}\right)^3$, where τ_e (the *entanglement time*, see Sec. III D) corresponds to the relaxation time scale of polymer strands of contour length = L_e. With *bulk* viscosity

$\eta_{\rm bulk} \approx \frac{\kappa_B T}{d_T^2 \xi} \tau_{\rm rep}$, at larger times nanoprobe motion becomes diffusive again

$$\langle \Delta r^2(\tau) \rangle_{\rm lin} \approx \frac{\kappa_B T}{\eta_{\rm bulk}\, d}\, \tau \approx \frac{\xi}{d}\, d_T^2 \left(\frac{L_c}{L_e}\right)^{-3} \frac{\tau}{\tau_e}. \tag{9}$$

C. Nanoprobe motion: Solutions of ring polymers

On length scales smaller than the tube diameter $d_T \approx (\ell_K L_e)^{1/2}$, ring and linear polymers behave similarly [see Eq. (1)], so dynamics of nanoprobes of small and intermediate sizes $d \lesssim d_T$ is described by the same expressions derived for nanoprobes immersed in linear chains, Eqs. (7) and (8).

Conversely, for nanoprobes with diameters $\gtrsim d_T$, dynamics at time scales $\gtrsim \tau_{d_T}$ reflects the different spatial organization of rings compared to linear polymers (Sec. II A). In this case, the time-dependent friction of the solution[49] $\eta = \eta(\tau) \approx \tau G(\tau)$. $G(\tau) \approx \frac{\kappa_B T}{b^2 L_e} \left(\frac{\tau}{\tau_e}\right)^{-\alpha}$ is the power-law stress relaxation modulus expected for rings in entangled solutions and b is the monomer linear size,[25] and it corresponds to the simultaneous rearrangement of polymer strands of contour length $L(\tau) \approx L_e \left(\frac{\tau}{\tau_e}\right)^{\alpha}$. The time MSD of the nanoprobe is thus given by

$$\langle \Delta r^2(\tau) \rangle_{\rm ring} \approx \frac{\kappa_B T}{\eta(\tau) d}\, \tau \approx \frac{b^2 L_e}{d} \left(\frac{\tau}{\tau_e}\right)^{\alpha}. \tag{10}$$

The regime breaks down at $\tau_d' \approx \tau_e \left(\frac{d}{d_T}\right)^{3/\alpha}$, namely, at the relaxation time of a polymer strand of spatial extension $\approx d$ in the compact regime [Eq. (3)]. Above τ_d', the nanoprobe is diffusive with MSD

$$\langle \Delta r^2(\tau) \rangle_{\rm ring} \approx \frac{\kappa_B T}{\eta(\tau_d') d}\, \tau \approx \frac{b^2 L_e}{d} \left(\frac{d}{d_T}\right)^{3(1-1/\alpha)} \frac{\tau}{\tau_e}. \tag{11}$$

With $\alpha \approx 0.4$,[25] Eqs. (9) and (11) for diffusional motions in solutions of linear *vs.* ring polymers suggest that, already at moderate ratios $L_c/L_e > 1$, nanoprobes diffuse much faster in the latter case than in the former.

III. MODEL AND METHODS

A. The model

Polymer model—To model solutions of dilute nanoprobes and linear and ring polymers at various monomer densities, we employ the same numerical framework considered in our previous studies[15,46] consisting of a variant of the known Kremer and Grest[52] polymer model.

Excluded volume interactions between beads (including consecutive ones along the contour of the chains) are modelled by the shifted and truncated Lennard-Jones (LJ) potential

$$U_{\rm LJ}(r) = \begin{cases} 4\epsilon \left[\left(\frac{\sigma}{r}\right)^{12} - \left(\frac{\sigma}{r}\right)^{6} + \frac{1}{4} \right] & r \le r_c \\ 0 & r > r_c \end{cases}, \tag{12}$$

where r denotes the separation between the bead centers. The cutoff distance $r_c = 2^{1/6}\sigma$ is chosen so that only the repulsive part of the Lennard-Jones is used. The energy scale is set by $\epsilon = \kappa_B T$ and the length scale is set by σ, both of which are set to unity in our simulations. Consistent with that, in this work all quantities are reported in reduced LJ units.

Nearest-neighbour monomers along the contour of the chains are connected by the finitely extensible nonlinear elastic (FENE) potential, given by

$$U_{\rm FENE}(r) = \begin{cases} -0.5 k R_0^2 \ln\left(1 - (r/R_0)^2\right) & r \le R_0 \\ \infty & r > R_0 \end{cases}, \tag{13}$$

where $k = 30\epsilon/\sigma^2$ is the spring constant and $R_0 = 1.5\sigma$ is the maximum extension of the elastic FENE bond.

In order to maximize mutual chain interpenetration at relatively moderate chain length[23] and hence reduce the computational effort, we have introduced an additional bending energy penalty between consecutive triplets of neighbouring beads along the chains in order to control polymer stiffness

$$U_{\rm bend}(\theta) = k_\theta \left(1 - \cos\theta\right). \tag{14}$$

Here, θ is the angle formed between adjacent bonds and $k_\theta = 5\kappa_B T$ is the bending constant. With this choice, the polymer is equivalent to a worm-like chain with Kuhn length $\ell_K = 10\sigma$.[53]

Nanoprobe model—Nanoprobe-monomer and nanoprobe-nanoprobe interactions are described by the model potentials introduced by Everaers and Ejtehadi.[54]

The total interaction energy between probes at center-to-center distance r can be represented as the sum of two functions

$$U_{\rm cc}(r) = \begin{cases} U_{\rm cc}^A(r) + U_{\rm cc}^R(r) & r \le r_{cc} \\ 0 & r > r_{\rm cc} \end{cases}. \tag{15}$$

$U_{\rm cc}^A(r)$ is the attractive component and it is given by

$$U_{\rm cc}^A(r) = -\frac{A_{\rm cc}}{6} \left[\frac{2a^2}{r^2 - 4a^2} + \frac{2a^2}{r^2} + \ln\left(\frac{r^2 - 4a^2}{r^2}\right) \right]. \tag{16}$$

The repulsive component of the interaction, $U_{\rm pp}^R(r)$, is

$$U_{\rm cc}^R(r) = \frac{A_{\rm cc}}{37800} \frac{\sigma^6}{r} \left[\frac{r^2 - 14ar + 54a^2}{(r-2a)^7} + \frac{r^2 + 14ar + 54a^2}{(r+2a)^7} - 2\frac{r^2 - 30a^2}{r^7} \right], \tag{17}$$

where[54] $A_{\rm cc} = 39.478\ k_B T$. We have considered non-sticky, athermal probe particles with diameters $d/\sigma \equiv 2a/\sigma = 2.5$, 5.0, 7.5 which correspond to truncating the interaction $U_{\rm cc}(r)$ to $r_{\rm cc}/\sigma = 3.08, 5.60, 8.08$. The smallest probe is comparable to or larger than the smallest polymer correlation length $\xi \lesssim 2.3\sigma$ (Table I), meaning that all probes are on or above length scales where polymer effects become dominant (Sec. II).

Finally, the interaction potential, $U_{\rm mc}$, between a single monomer and a nanoprobe with center-to-center distance r is given by

$$U_{\rm mc}(r) = \begin{cases} \frac{2a^3\sigma^3 A_{\rm mc}}{9(a^2 - r^2)^3} \left[1 - \frac{(5a^6 + 45a^4 r^2 + 63a^2 r^4 + 15r^6)\sigma^6}{15(a-r)^6 (a+r)^6} \right] & r \le r_{\rm mc} \\ 0 & r \ge r_{\rm mc} \end{cases}, \tag{18}$$

where[54] $A_{\rm mc} = 75.358\ k_B T$. According to our choices of probe diameters, the interaction $U_{\rm mc}(r)$ is truncated to $r_{\rm mc}/\sigma = 2.11$, 3.36, 4.61.

TABLE I. Summary of the physical properties of polymer solutions and diffusing nanoprobes as functions of solution density expressed in monomer (ρ) or Kuhn segment (ρ_K) units: (a) L_e, entanglement length. (b) d_T, tube diameter. (c) τ_e, entanglement time. (d) d, nanoprobe diameter. (e) ξ, correlation length. (f) D, terminal diffusion coefficient of dispersed nanoprobes obtained by averaging the results of linear fits to single-nanoprobe displacements for lag-times $\tau > 100\tau_e$. Error bars correspond to standard deviations.

						Linear polymers		Ring polymers	
$\rho\sigma^3$	$\rho_K\ell_K^3$	L_e/σ [Eq. (19)]	d_T/σ [Eq. (20)]	τ_e/τ_{MD}	d/σ	ξ/σ	D [σ^2/τ_{MD}]	ξ/σ	D [σ^2/τ_{MD}]
0.1	10	40.0	8.2	≈1600	2.5	2.1	$(4.73 \pm 2.33) \times 10^{-1}$	2.3	$(4.91 \pm 2.36) \times 10^{-1}$
					5.0		$(1.28 \pm 0.72) \times 10^{-1}$		$(1.23 \pm 0.63) \times 10^{-1}$
					7.5		$(3.18 \pm 1.59) \times 10^{-2}$		$(3.37 \pm 1.37) \times 10^{-2}$
0.2	20	16.2	5.2	≈570	2.5	1.6	$(1.51 \pm 0.84) \times 10^{-1}$	1.7	$(1.60 \pm 0.75) \times 10^{-1}$
					5.0		$(2.46 \pm 1.28) \times 10^{-2}$		$(3.22 \pm 1.60) \times 10^{-2}$
					7.5		$(2.82 \pm 1.32) \times 10^{-3}$		$(7.91 \pm 3.83) \times 10^{-3}$
0.3	30	11.0	4.3	≈490	2.5	1.4	$(6.24 \pm 3.13) \times 10^{-2}$	1.4	$(6.62 \pm 3.28) \times 10^{-2}$
					5.0		$(6.24 \pm 3.04) \times 10^{-3}$		$(1.25 \pm 0.56) \times 10^{-2}$
					7.5		$(7.67 \pm 6.17) \times 10^{-5}$		$(2.66 \pm 1.12) \times 10^{-3}$
0.4	40	8.8	3.8	≈540	2.5	1.3	$(2.57 \pm 1.21) \times 10^{-2}$	1.3	$(2.93 \pm 1.58) \times 10^{-2}$
					5.0		$(1.94 \pm 1.03) \times 10^{-3}$		$(4.92 \pm 2.49) \times 10^{-3}$
					7.5		$(1.75 \pm 1.55) \times 10^{-6}$		$(7.13 \pm 3.64) \times 10^{-4}$

B. Simulation details

As in our former work,[15] we consider polymer solutions consisting of $M = 80$ circular or linear chains made of $N_m = 500$ monomers each. The total number of monomers is then fixed to 40 000 monomer units. Each polymer solution includes also $N_{np} = 100$ nanoprobes of diameters $d/\sigma = 2.5, 5.0, 7.5$. These values were suitably chosen to cover the range from below to above the tube diameters of the polymer solutions (see Sec. III D). The volumes of the simulation box *accessible* to chain monomers have been chosen in order to explore monomer densities $\rho\sigma^3 = 0.1, 0.2, 0.3, 0.4$, corresponding, respectively, to Kuhn segment densities $\rho_K\ell_K^3 = 10, 20, 30, 40$.

The static and kinetic properties of chains and nanoprobes are studied using fixed-volume and constant-temperature Molecular Dynamics (MD) simulations with implicit solvent and periodic boundary conditions. MD simulations are performed using the LAMMPS package.[55] The equations of motion are integrated using a velocity Verlet algorithm, in which all beads are weakly coupled to a Langevin heat bath with a local damping constant $\Gamma = 0.5\tau_{MD}^{-1}$, where $\tau_{MD} = \sigma(m/\epsilon)^{1/2}$ is the Lennard-Jones time and $m = 1$ is the conventional mass unit for monomer and colloidal probes. The integration time step is set to $\Delta t = 0.012\tau_{MD}$.

The length of each MD run is equal to $2.4 \times 10^7\tau_{MD}$, during which (see the supplementary material of Ref. 15) each polymer moves on average of a spatial distance larger than its own average size or gyration radius R_g.

C. Choice of initial configurations and check for equilibration

At any given ρ, we started from the *equilibrated* polymer solutions made of $M \times N_m = 80 \times 500$ monomers and $N_{np} = 100$ dilute nanoprobes of diameter $d/\sigma = 5.0$ described in our previous publication.[15] With no modifications, those configurations have been used as the starting configurations for MD runs with the same probe diameter. For simulations with probe diameter of $d/\sigma = 2.5$, we have simply replaced the former probes by the corresponding smaller ones and proceeded to compress the simulation box slightly, in order to work at the same monomer densities. Sticking into the same logic, for simulations with larger probe diameter $d/\sigma = 7.5$, we have proceeded to inflate simultaneously the probes and the simulation box. We have accomplished this task by performing short (of the order of a few tens of τ_{MD}'s) MD runs with a soft (i.e., non-diverging), capped repulsive interaction between chain monomers and probes. At the end of these preparatory runs, we have checked the perturbation of chains' conformations after the deflation/inflation steps by measuring[53] the mean-square internal distances, $\langle R^2(L)\rangle$, between pairs of monomers at contour length separation L, see Fig. 1. The perfect agreement between different curves at each density demonstrates that the probes have perturbed in no sensible manner the overall chains' conformations.

D. Estimating entanglement length (L_e), tube diameter (d_T), and entanglement time (τ_e)

As briefly mentioned in Sec. II A, topological constraints confine the motion of any given linear chain to a tube-like region of diameter d_T. The contour length of sub-chains spanning a region of linear size = d_T and the associated diffusion time define, respectively, the entanglement length, L_e, and the entanglement time, τ_e.

As in our previous studies,[15,32,56] all these quantities can be estimated by employing the results by Uchida *et al.*[57] The entanglement length, L_e, is given by the following function of the polymer Kuhn length, ℓ_K, and the density of Kuhn segments, ρ_K:

$$\frac{L_e}{\ell_K} = \frac{1}{(0.06(\rho_K\ell_K^3))^{2/5}} + \frac{1}{(0.06(\rho_K\ell_K^3))^2}. \quad (19)$$

Accordingly, the tube diameter is defined[48,58] as the average gyration radius of a *linear* chain of contour length L_e

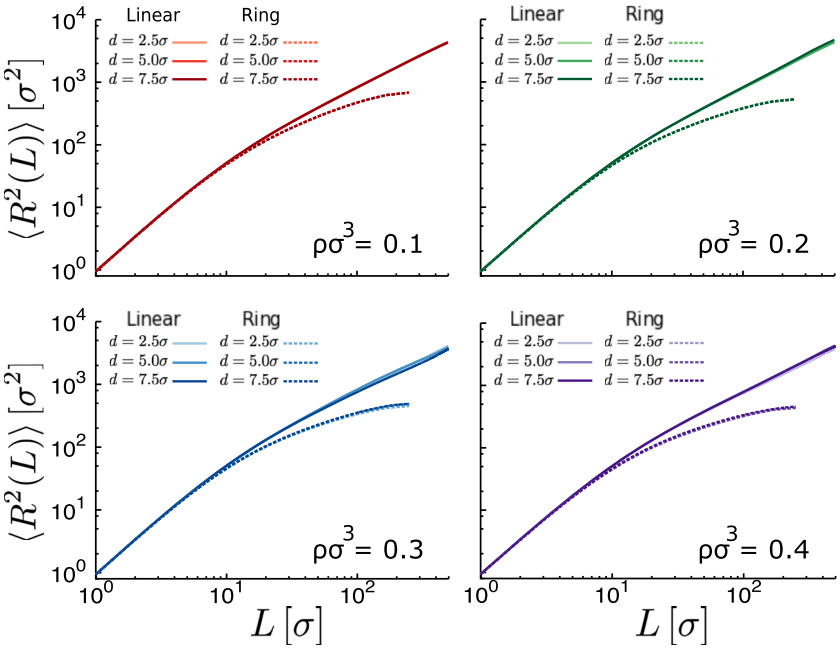

FIG. 1. Mean-square internal distances, $\langle R^2(L)\rangle$, between pair of monomers at contour length separation L: results for linear chains (solid lines) and ring polymers (dashed lines). Averages have been calculated on the first parts of the corresponding MD trajectories, immediately after the introduction of the nanoprobes.

$$d_T = \sqrt{\frac{\ell_K L_e}{6}}. \tag{20}$$

Finally, the entanglement time (τ_e) was estimated from the monomer mean-square displacement, $\langle g_1(\tau)\rangle$, at lag-time τ by using[48,58] $\langle g_1(\tau_e)\rangle = 2d_T^2$. As for nanoprobe displacement $\langle \delta r^2(\tau)\rangle$ (Sec. II B), $\langle g_1(\tau)\rangle$ is both time- and ensemble-averaged

$$\langle g_1(\tau)\rangle \equiv \frac{1}{M\times N_m}\sum_{i=1}^{M\times N_m}\lim_{\mathcal{T}\to\infty}\frac{1}{\mathcal{T}-\tau} \times \int_0^{\mathcal{T}-\tau}(\vec{r}_i(t+\tau)-\vec{r}_i(t))^2 dt \tag{21}$$

with $\vec{r}_i(t)$ being the spatial coordinate of monomer i at time t.

L_e, d_T, and τ_e have been calculated for our solutions of linear chains at different Kuhn densities ρ_K and summarized in Table I. For the sake of comparison, the same values have been applied to ring polymers.

IV. RESULTS

A. Nanoprobe diffusion in entangled polymer solutions: Average properties

In order to study the influence of chain architecture on the diffusion of nanoprobes dispersed in polymer solutions, we consider their time- *and* ensemble-averaged displacement $\langle \Delta r^2(\tau)\rangle$ at lag-time τ (see Sec. II B for definition). We employ the notation $\langle \Delta r^2(\tau)\rangle_{\rm lin}$ (respectively, $\langle \Delta r^2(\tau)\rangle_{\rm ring}$) for solutions of linear (respectively, ring) polymers.

Results are shown in Fig. 2, with the horizontal and vertical axes scaled down by units of entanglement times τ_e and tube diameters d_T (Table I), respectively. Insets show the corresponding ratios of MSDs for unconcatenated rings' solutions *vs.* linear chains' solutions. Figure 3 shows results for the corresponding time local exponents, $\alpha(\tau)$, defined as $\alpha(\tau) \equiv \frac{d\log\langle \Delta r^2(\tau)\rangle}{d\log\tau}$, which provides a direct visualization of those regimes where diffusion markedly deviates from standard Brownian motion (i.e., $\alpha = 1$).

By comparing the results for different densities ρ (or, tube diameters d_T) and probe diameters d, we may clearly distinguish two regimes: (1) for $d < d_T$, entanglements have no effect on probe diffusion which looks almost identical for solutions of linear and ring polymers. Moreover, at short times $\langle \Delta r^2(\tau)\rangle \sim \tau^\alpha$ with α approaching 1/2 suggesting coupling of nanoprobe motion to the Rouse modes of the chains; (2) conversely, for $d > d_T$, nanoprobe diffusion is markedly slower in solutions of linear chains compared to rings. This is particularly evident in the "$\rho\sigma^3 = 0.4$"-panel in Fig. 2 and nanoprobe diameter $d = 7.5\sigma$. Here, nanoprobes in rings' solutions shift from anomalous to normal diffusion at about τ_e, while the same probes in solutions of linear chains show a longer subdiffusive behavior with a smaller scaling exponent (see the corresponding panel in Fig. 3). Then, normal terminal diffusion is characterized by a $\approx 400\times$ smaller diffusion coefficient, D (Table I).

In general, these results are in qualitative agreement with the theory by Ge *et al.* summarized in Secs. II B and II C. More quantitatively, it is instructive to compare the ratio of terminal diffusion coefficient for linear chains and rings predicted by Eqs. (9) and (11), respectively. We consider again the case of $\rho\sigma^3 = 0.4$ and nanoprobe diameter $d = 7.5\sigma$. By using data reported in Table I with polymer diameter $b/\sigma \approx 1$, we get $\lim_{\tau\to\infty}\langle \Delta r^2(\tau)\rangle_{\rm ring}/\langle \Delta r^2(\tau)\rangle_{\rm lin} \approx 4\times 10^3$. This is $\approx 10\times$ our numerical estimate. Several factors may be advocated, which may explain this discrepancy. First, Eqs. (9) and (11) are not exact but systematically neglect unknown prefactors. Second (and equally important), as it was pointed out by Ge *et al.*[14] "hopping" between close-by entanglements may enhance nanoprobe diffusion in solutions of linear chains, which, in turn, may lead to better agreement with numerical simulations.

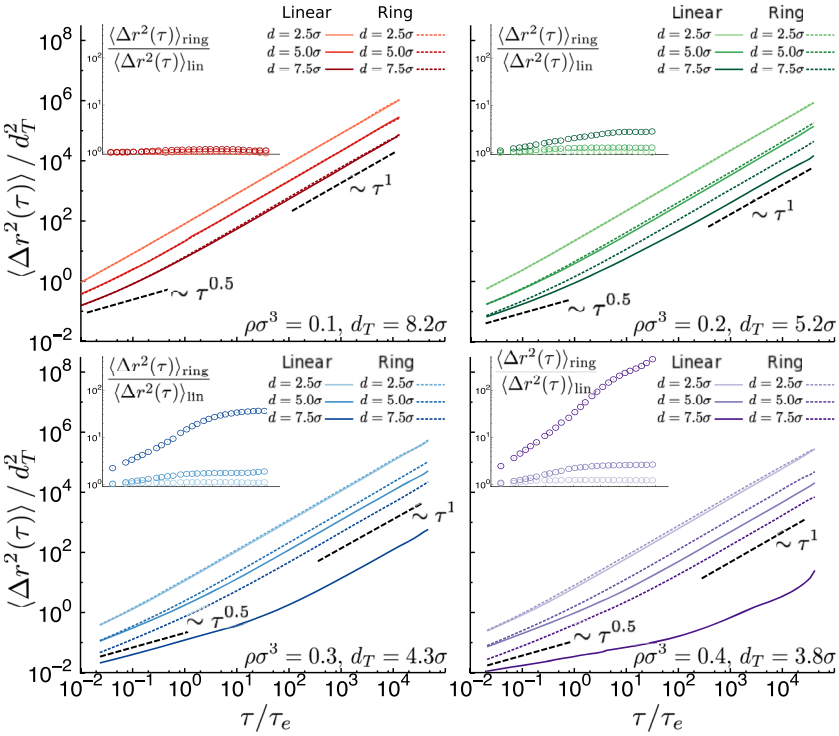

FIG. 2. Mean-square displacements as functions of lag-time τ for nanoprobes of diameters d/σ = 2.5, 5.0, 7.5: results for entangled solutions of linear polymers ($\langle\Delta r^2(\tau)\rangle_{\rm lin}$, solid lines) and unconcatenated ring polymers ($\langle\Delta r^2(\tau)\rangle_{\rm ring}$, dashed lines). Insets: corresponding ratios $\langle\Delta r^2(\tau)\rangle_{\rm ring}/\langle\Delta r^2(\tau)\rangle_{\rm lin}$. Probes of diameter d larger than the tube diameter d_T of the corresponding polymer solution diffuse markedly faster in rings' systems. Color code and symbols are as in Fig. 1.

On the other hand, there is more to nanoprobe motion that cannot be captured by just its mean-square displacement: in Sec. IV B, we will discuss the statistical properties of *distribution functions* for several selected observables which provide a far more vivid description of nanoprobe behavior.

B. Nanoprobe diffusion in entangled polymer solutions: Distribution functions

In order to characterize nanoprobe dynamics beyond the MSD, we introduce the probability distribution functions $P(\tau;\ \Delta x) \equiv \langle(\Delta x - (x(t+\tau) - x(t)))\rangle$ of *one-dimensional* displacements Δx for a given lag-time τ. $P(\tau;\ \Delta x)$ corresponds to the self-part of the so-called van-Hove function,[59] and it measures the probability that a probe reaches the spatial position $x(t+\tau)$ from $x(t)$ after time τ. Thus, while $\langle\Delta r^2(\tau)\rangle = 3\langle\Delta x^2(\tau)\rangle$ is just proportional to the second moment of $P(\tau;\ \Delta x)$, the detailed knowledge of $P(\tau;\ \Delta x)$ gives deeper insight for the whole diffusion process.

To fix the ideas, we have considered the three representative lag-times $\tau/\tau_e = 10^{-1}, 10^0, 10^3$. Results are illustrated

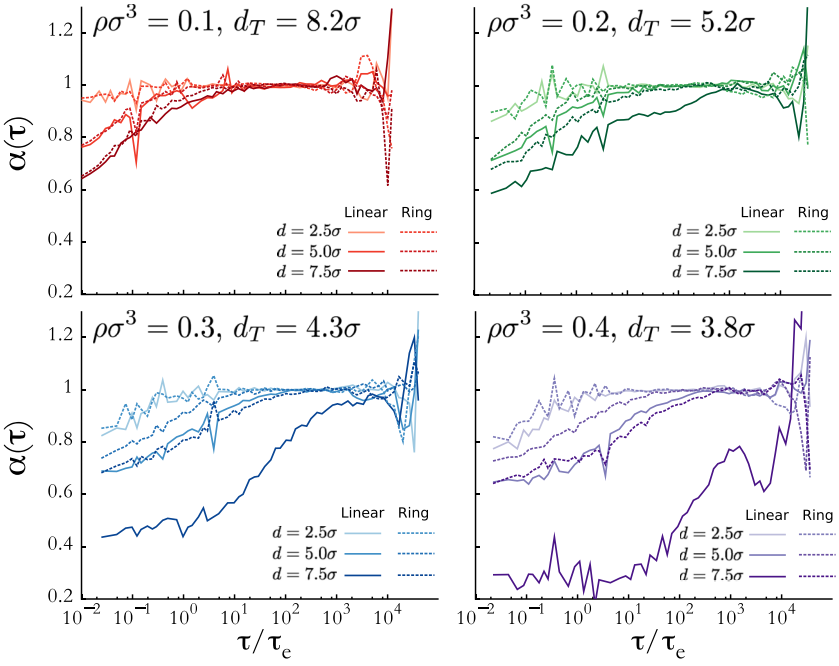

FIG. 3. Time-dependent differential exponents of nanoprobe mean square displacements, $\alpha(\tau) \equiv \frac{d\log\langle\Delta r^2(\tau)\rangle}{d\log\tau}$. Color code and symbols are as in Fig. 1.

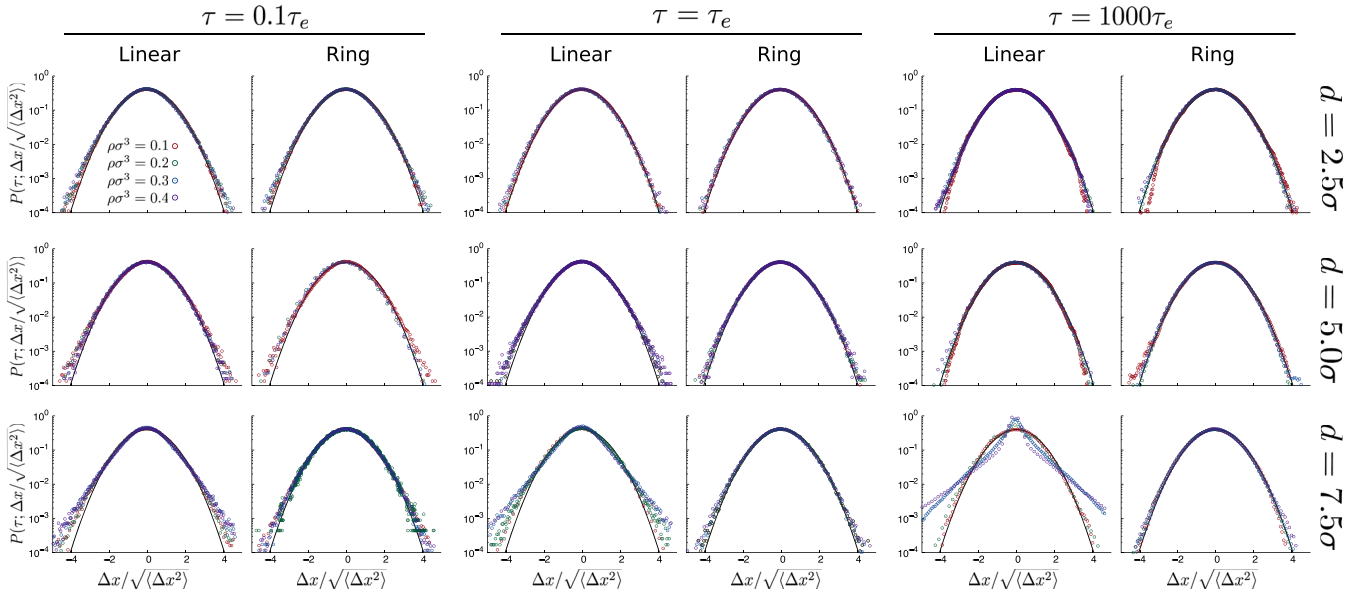

FIG. 4. Probability distribution functions of one-dimensional nanoprobe displacements, $P(\tau;\Delta x)$, for lag-time τ. Representative curves for given polymer solution density ρ, nanoprobe diameter d, and lag-time τ. The black solid line in each panel corresponds to the Gaussian distribution. Color code is as in Fig. 1.

in Fig. 4 where, in order to ease visualization between different lag-times, horizontal axes have been scaled to the square root of the corresponding second moment, $\sqrt{\langle\Delta x^2(\tau)\rangle}$ and the curves compared to the universal Gaussian curve $P(\tau;\Delta x) = P(\Delta x) = \sqrt{\frac{1}{2\pi\langle\Delta x^2\rangle}}\exp(-\frac{\Delta x^2}{2\langle\Delta x^2\rangle})$ (black solid lines).

Interpretation of results appears thus straightforward: with the notable exception of nanoprobes of diameter = 7.5σ, distributions are always or almost Gaussian. Tiny deviations from Gaussian behavior can be seen at the shortest lag-time and should be ascribed to the coupling of nanoprobes with the Rouse modes of the chains. Unperturbed Gaussian behavior is also observed for large nanoprobes in rings' solutions at *any* density.

Intriguingly, the case of large ($d = 7.5\sigma$, bottom row) nanoprobes in solutions of linear chains appears far from trivial. For low-density solutions, nanoprobes remain Gaussian. Conversely, for the highest densities $\rho\sigma^3 = 0.3, 0.4$, we observe (1) a more pronounced peak around $\Delta x = 0$ and (2) the appearance of "fat", exponential tails which become increasingly evident at large lag-times.

The rationale behind the highest peak is the following: nanoprobe dynamics is hindered by the presence of entanglements arising from surrounding polymers which act as "cages". In order to quantify this further, we consider[6] the distribution function $P(\tau;\theta) \equiv \langle\theta - \cos^{-1}\left(\frac{(\vec{r}(t+\tau)-\vec{r}(t))\cdot(\vec{r}(t+2\tau)-\vec{r}(t+\tau))}{|\vec{r}(t+\tau)-\vec{r}(t)|\,|\vec{r}(t+2\tau)-\vec{r}(t+\tau)|}\right)\rangle$ of angles θ between spatial

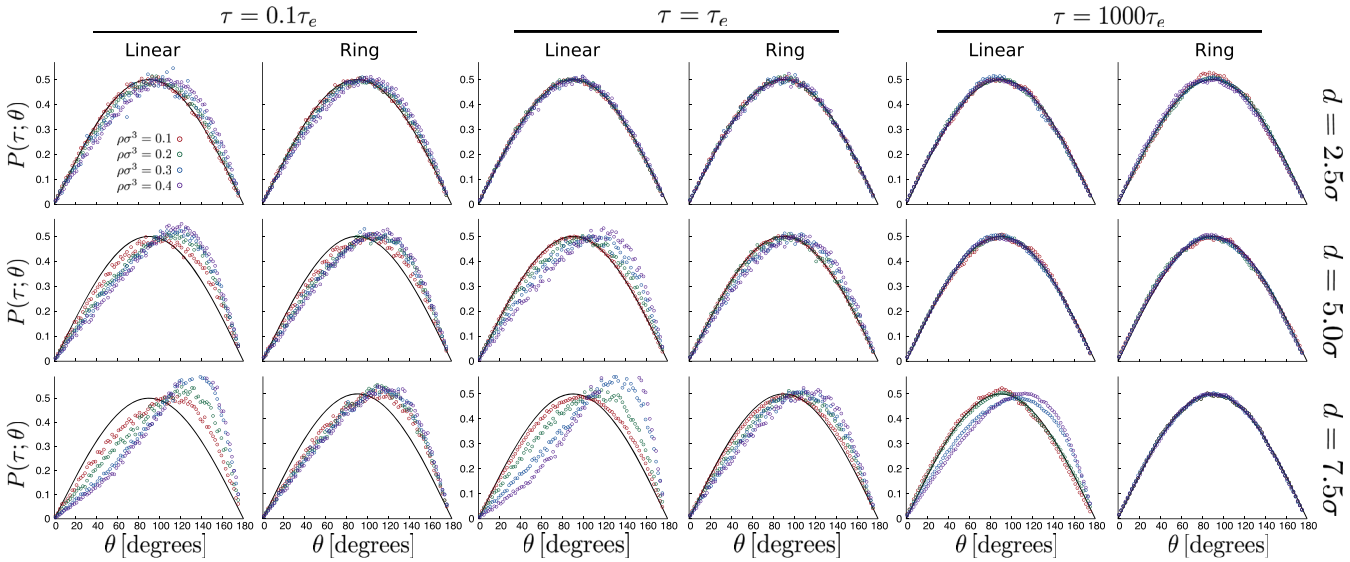

FIG. 5. Probability distribution function, $P(\tau;\theta)$, of angles θ between spatial orientations of pairs of nanoprobe displacements separated by lag-time τ. Representative curves for given polymer solution density ρ, nanoprobe diameter d and lag-time τ (as in Fig. 4). The black solid line in each panel corresponds to the "random" distribution $P(\theta) = \sin(\theta)/2$. Color code is as in Fig. 1.

orientations of pairs of nanoprobe displacements separated by lag-time τ. For random displacements, we expect that $P(\tau;\theta) = \sin(\theta)/2$. Caged particles, instead, are expected to be skewed toward $\theta > \pi/2$. These predictions get confirmed by the plots shown in Fig. 5 representing distribution functions $P(\tau;\theta)$ corresponding to the same lag-times as in Fig. 4. Particularly pronounced is the difference between distributions observed in solutions of linear chains *vs.* rings with large nanoprobes (bottom row), a vivid signature of the different role of entanglements in the two systems. Deviations from the "random" distribution are also observable in rings' solutions; however, they appear overall "less persistent" in time than for solutions of linear chains.

The presence of exponential tails in the van-Hove function has been reported long ago[50] in connection to single-particle dynamics in glassy and jammed systems. Recently, we have shown[46] that this property characterizes also the dynamics of unconcatenated rings in high-density solutions, while linear chains remain Gaussian. Simultaneously, in that work we have demonstrated that topological constraints between close-by rings tend to cluster the polymers into distinct sub-populations with definite diffusivities, thus triggering non-ergodic heterogeneous dynamics.

To verify if anything similar applies to nanoprobe dynamics as well and in order to better understand their deviations from Gaussian behavior, we consider[46] the ratio

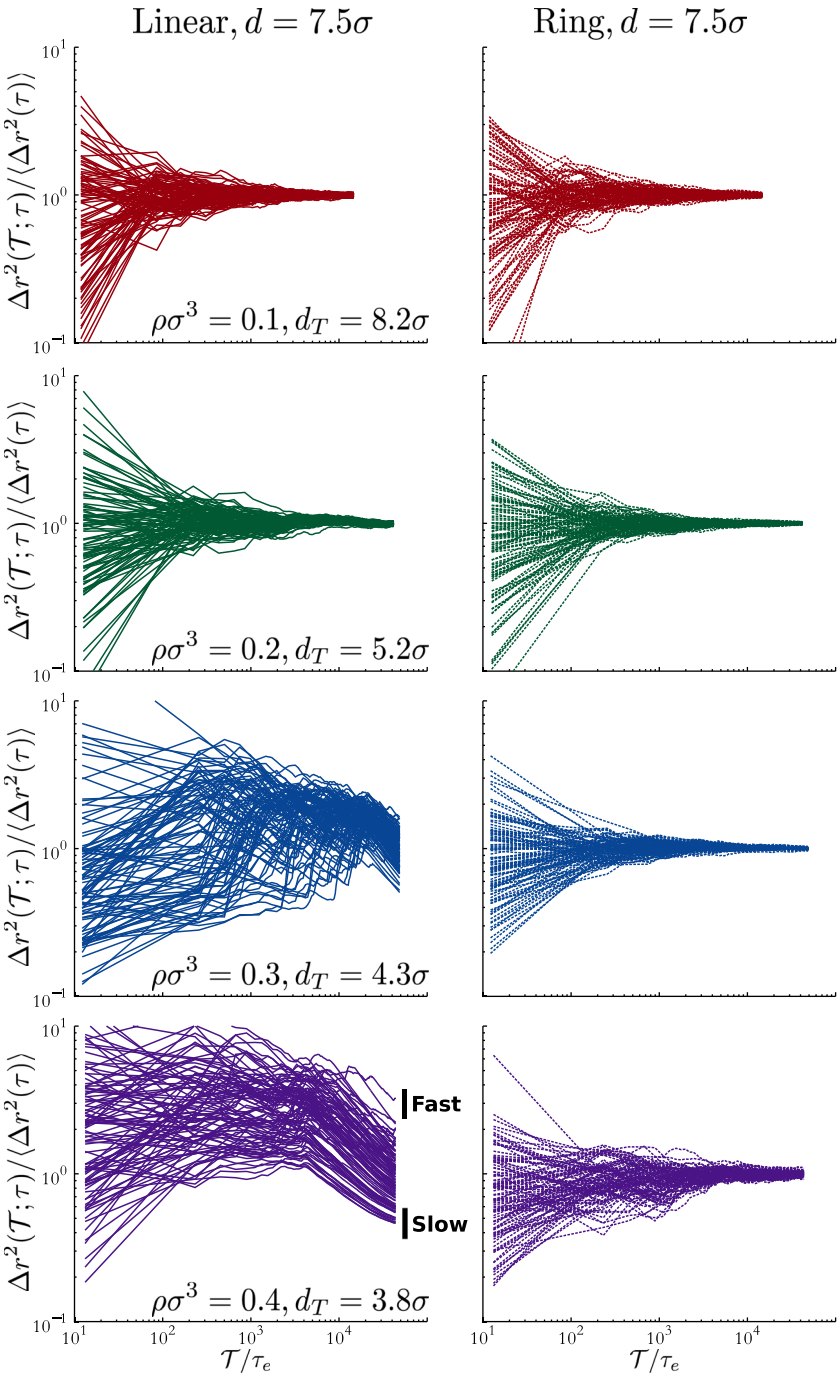

FIG. 6. Spatial heterogeneity of displacements $\Delta r^2(\mathcal{T};\tau)/\langle\Delta r^2(\tau)\rangle$ of nanoprobes of diameter $d = 7.5\sigma$ as a function of measurement time $\mathcal{T}$ and lag-time $\tau/\tau_e = 10$. At high densities, nanoprobe dynamics becomes heterogeneous alternating slow to fast trajectories. Color code and symbols are as in Fig. 1.

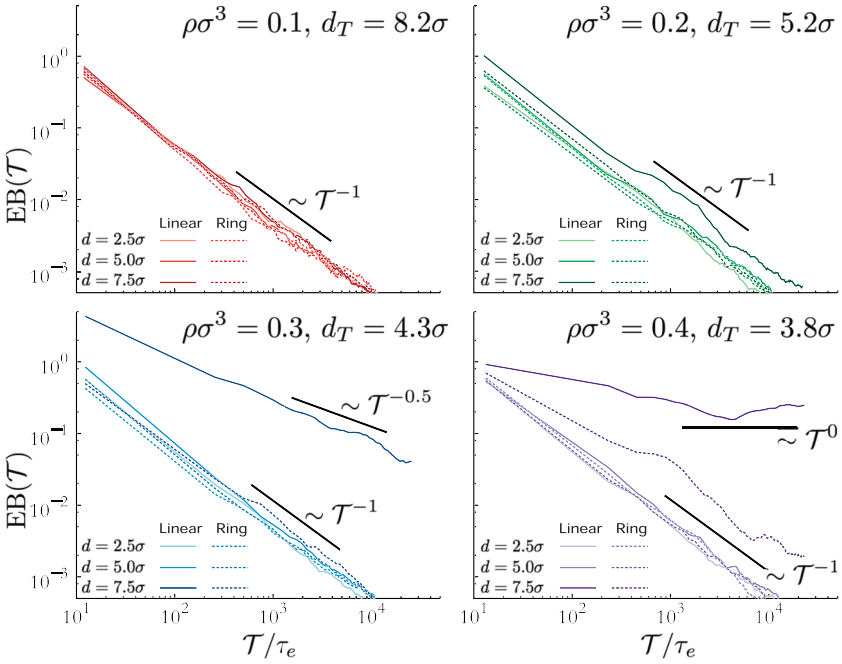

FIG. 7. Ergodicity-breaking (EB) parameter [Eq. (22)] as a function of measurement time $\mathcal{T}$ and lag-time $\tau/\tau_e = 10$. EB($\mathcal{T}$) $\sim \mathcal{T}^{-1}$ marks standard diffusive processes, whereas EB($\mathcal{T}$) $\sim \mathcal{T}^0$ is a signature of ergodicity breaking. Color code and symbols are as in Fig. 1.

$\Delta r^2(\mathcal{T};\tau)/\langle\Delta r^2(\tau)\rangle$ as a function of measurement time $\mathcal{T}$ and fixed lag-time τ. Figure 6 shows representative curves for the largest nanoprobes ($d = 7.5\sigma$) in solutions of linear and ring polymers. Thus, while Gaussian behavior implies that the curves converge to the corresponding average value, non-Gaussian nanoprobes in high-density solutions of linear chains (see Fig. 4) alternate between slow to fast trajectories and are thus characterized by heterogeneous dynamics. Then, to quantify relaxation to equilibrium and ergodicity breaking (EB), we introduce the so-called *ergodicity-breaking* (EB) parameter[46,60]

$$EB(\mathcal{T}) = \frac{\langle(\Delta r^2(\mathcal{T};\tau))^2\rangle}{\langle\Delta r^2(\mathcal{T};\tau)\rangle^2} - 1, \tag{22}$$

which captures how fast the single-nanoprobe trajectories $\Delta r^2(\mathcal{T};\tau)$ narrow around the mean $\langle\Delta r^2(\tau)\rangle$ for some specific lag-time τ. For standard diffusive solutions, $EB(\mathcal{T})$ decays as[60] $\mathcal{T}^{-1}$, whereas in nonergodic systems[61] $EB(\mathcal{T}) \sim \mathcal{T}^0$. Indeed, Fig. 7 shows that topological constraints in systems of linear chains trigger ergodicity breaking of diffusive nanoprobes when the size of those exceeds the tube diameter of the solution. Inversely, we highlight that solutions of ring polymers do not induce anything similar and, thus, probe dynamics remains ergodic.

V. CONCLUSIONS AND OUTLOOK

In this work, we have employed large-scale computer simulations to investigate the physics of nanoprobe motion in polymer solutions of linear chains *vs.* unconcatenated ring polymers which represent the most simple, yet not trivial, examples of complex polymer systems where entanglements between close-by chains operate on polymer conformations in "distinct" manners: linear chains follow Gaussian statistics and strongly overlap with each other,[48] while ring polymers tend to crumple as space-filling objects.[31,32]

By tuning physical parameters like nanoprobe diameter and solution density, we have focused, in particular, on nanoprobe diffusion at the transition from the non-entangled to the entangled regime corresponding to nanoprobes smaller/larger than the tube diameter of the solution. We have thus confirmed and extended (Sec. IV A) recent[15,17] numerical results demonstrating that nanoprobes in rings' solutions diffuse faster than in the corresponding solutions of linear chains whenever nanoprobe size exceeds the tube diameter of the embedding solution, in agreement with the theoretical picture proposed recently by Ge *et al.* (Secs. II B and II C). Then, we have shown (Sec. IV B) that the corresponding distribution functions for spatial displacements markedly deviate from Gaussian statistics only in solutions of linear chains with nanoprobe motion turning to be *non-ergodic*. Conversely, nanoprobe motion in solutions of rings remains both Gaussian and ergodic.

In a recent publication,[46] we have demonstrated that "non-Gaussian/non-ergodic" dynamics is a characteristic trademark of self-diffusing rings in sufficiently dense solutions while linear chains follow conventional dynamics: this strikes as the opposite of the trend reported here for dispersed nanoprobes in the same media. At the same time, a consistent amount of theoretical and experimental studies (see, for instance, the recent studies[10,62]) have demonstrated that doping polymer solutions through the insertion of nanoprobes may enhance to a significant extent the mechanical property of the solution. As a follow-up of this work, it would be then interesting to quantify to which extent the presence of nanoprobes is able to alter the dynamical properties of the chains, especially rings in high-density solutions which appear to be characterized by heterogeneous dynamics. Second, future investigations should not be bound only to homogeneous solutions: notoriously, even a minimal amount of linear contaminants in solutions of ring polymers is able to enhance their mechanical response in

comparison to pure samples.[25] It would then be especially interesting to address nanoprobe diffusion in such mixed linear/ring polymer solutions.

ACKNOWLEDGMENTS

The authors acknowledge computational resources from SISSA HPC-facilities.

[1]T. G. Mason and D. A. Weitz, "Optical measurements of frequency-dependent linear viscoelastic moduli of complex fluids," Phys. Rev. Lett. **74**, 1250–1253 (1995).
[2]T. G. Mason, "Estimating the viscoelastic moduli of complex fluids using the generalized Stokes–einstein equation," Rheol. Acta **39**, 371–378 (2000).
[3]Y. Tseng, T. P. Kole, and D. Wirtz. "Micromechanical mapping of live cells by multiple-particle-tracking microrheology," Biophys. J. **83**, 3162–3176 (2002).
[4]T. A. Waigh, "Microrheology of complex fluids," Rep. Prog. Phys. **68**, 685 (2005).
[5]D. Wirtz, "Particle-tracking microrheology of living cells: Principles and applications," Annu. Rev. Biophys. **38**, 301–326 (2009).
[6]M. Valet and A. Rosa, "Viscoelasticity of model interphase chromosomes," J. Chem. Phys. **141**, 245101 (2014).
[7]T. A. Waigh, "Advances in the microrheology of complex fluids," Rep. Prog. Phys. **79**, 074601 (2016).
[8]W. Liu and C. Wu, "Rheological study of soft matters: A review of microrheology and microrheometers," Macromol. Chem. Phys. **219**, 1700307 (2017).
[9]R. A. Riggleman, G. Toepperwein, G. J. Papakonstantopoulos, J.-L. Barrat, and J. J. de Pablo, "Entanglement network in nanoparticle reinforced polymers," J. Chem. Phys. **130**, 244903 (2009).
[10]S. K. Kumar, V. Ganesan, and R. A. Riggleman, "Perspective: Outstanding theoretical questions in polymer-nanoparticle hybrids," J. Chem. Phys. **147**, 020901 (2017).
[11]F. Brochard Wyart and P. G. de Gennes, "Viscosity at small scales in polymer melts," Eur. Phys. J. E **1**, 93–97 (2000).
[12]L.-H. Cai, S. Panyukov, and M. Rubinstein, "Mobility of nonsticky nanoparticles in polymer liquids," Macromolecules **44**, 7853–7863 (2011).
[13]J. T. Kalathi, U. Yamamoto, K. S. Schweizer, G. S. Grest, and S. K. Kumar, "Nanoparticle diffusion in polymer nanocomposites," Phys. Rev. Lett. **112**, 108301 (2014).
[14]L.-H. Cai, S. Panyukov, and M. Rubinstein, "Hopping diffusion of nanoparticles in polymer matrices," Macromolecules **48**, 847–862 (2015).
[15]N. Nahali and A. Rosa, "Density effects in entangled solutions of linear and ring polymers," J. Phys.: Condens. Matter **28**, 065101 (2016).
[16]A. Y. Grosberg, J.-F. Joanny, W. Srinin, and Y. Rabin, "Scale-dependent viscosity in polymer fluids," J. Phys. Chem. B **120**, 6383–6390 (2016).
[17]T. Ge, J. T. Kalathi, J. D. Halverson, G. S. Grest, and M. Rubinstein, "Nanoparticle motion in entangled melts of linear and nonconcatenated ring polymers," Macromolecules **50**, 1749–1754 (2017).
[18]T. Ge, G. S. Grest, and M. Rubinstein, "Nanorheology of entangled polymer melts," Phys. Rev. Lett. **120**, 057801 (2018).
[19]A. R. Khokhlov and S. K. Nechaev, "Polymer chain in an array of obstacles," Phys. Lett. **112A**, 156–160 (1985).
[20]M. E. Cates and J. M. Deutsch, "Conjectures on the statistics of ring polymers," J. Phys. **47**, 2121–2128 (1986).
[21]A. Y. Grosberg, S. K. Nechaev, and E. I. Shakhnovich, "The role of topological constraints in the kinetics of collapse of macromolecules," J. Phys. France **49**, 2095–2100 (1988).
[22]S. P. Obukhov, M. Rubinstein, and T. Duke, "Dynamics of a ring polymer in a gel," Phys. Rev. Lett. **73**, 1263–1266 (1994).
[23]M. Müller, J. P. Wittmer, and M. E. Cates, "Topological effects in ring polymers. II. influence of persistence length," Phys. Rev. E **61**, 4078–4089 (2000).
[24]T. C. B. McLeish, "Floored by the rings," Nature **7**, 933–935 (2008).
[25]M. Kapnistos, M. Lang, D. Vlassopoulos, W. Pyckhout-Hintzen, D. Richter, D. Cho, T. Chang, and M. Rubinstein, "Unexpected power-law stress relaxation of entangled ring polymers," Nat. Mater. **7**, 997 (2008).
[26]J. Suzuki, A. Takano, T. Deguchi, and Y. Matsushita, "Dimension of ring polymers in bulk studied by Monte-Carlo simulation and self-consistent theory," J. Chem. Phys. **131**, 144902 (2009).
[27]J. D. Halverson, W. B. Lee, G. S. Grest, A. Y. Grosberg, and K. Kremer, "Molecular dynamics simulation study of nonconcatenated ring polymers in a melt. I. Statics," J. Chem. Phys. **134**, 204904 (2011).
[28]J. D. Halverson, W. B. Lee, G. S. Grest, A. Y. Grosberg, and K. Kremer, "Molecular dynamics simulation study of nonconcatenated ring polymers in a melt. II. Dynamics," J. Chem. Phys. **134**, 204905 (2011).
[29]A. Rosa, E. Orlandini, L. Tubiana, and C. Micheletti, "Structure and dynamics of ring polymers: Entanglement effects because of solution density and ring topology," Macromolecules **44**, 8668–8680 (2011).
[30]T. Sakaue, "Ring polymers in melts and solutions: Scaling and crossover," Phys. Rev. Lett. **106**, 167802 (2012).
[31]A. Y. Grosberg, "Annealed lattice animal model and flory theory for the melt of non-concatenated rings: Towards the physics of crumpling," Soft Matter **10**, 560–565 (2014).
[32]A. Rosa and R. Everaers, "Ring polymers in the melt state: The physics of crumpling," Phys. Rev. Lett. **112**, 118302 (2014).
[33]S. Gooßen, A. R. E. Brás, M. Krutyeva, M. Sharp, P. Falus, A. Feoktystov, U. Gasser, A. Wischnewski, and D. Richter, "Molecular scale dynamics of large ring polymers," Phys. Rev. Lett. **113**, 169302 (2014).
[34]A. R. Brás, S. Gooßen, M. Krutyeva, A. Radulescu, B. Farago, J. Allgaier, W. Pyckhout-Hintzen, A. Wischnewski, and D. Richter, "Compact structure and non-Gaussian dynamics of ring polymer melts," Soft Matter **10**, 3649–3655 (2014).
[35]S. Gooßen, M. Krutyeva, M. Sharp, A. Feoktystov, J. Allgaier, W. Pyckhout-Hintzen, A. Wischnewski, and D. Richter, "Sensing polymer chain dynamics through ring topology: A neutron spin echo study," Phys. Rev. Lett. **115**, 148302 (2015).
[36]D. Richter, S. Gooßen, and A. Wischnewski, "Celebrating soft matter's 10th anniversary: Topology matters: Structure and dynamics of ring polymers," Soft Matter **11**, 8535–8549 (2015).
[37]D. Vlassopoulos, "Macromolecular topology and rheology: Beyond the tube model," Rheol. Acta **55**, 613–632 (2016).
[38]D. Michieletto, D. Marenduzzo, E. Orlandini, G. P. Alexander, and M. S. Turner, "Threading dynamics of ring polymers in a gel," ACS Macro Lett. **3**(3), 255–259 (2014).
[39]D. G. Tsalikis and V. G. Mavrantzas, "Threading of ring poly(ethylene oxide) molecules by linear chains in the melt," ACS Macro Lett. **3**, 763–766 (2014).
[40]J. Smrek and A. Y. Grosberg, "Understanding the dynamics of rings in the melt in terms of the annealed tree model," J. Phys.: Condens. Matter **27**, 064117 (2015).
[41]E. Lee, S. Kim, and Y. Jung, "Slowing down of ring polymer diffusion caused by inter-ring threading," Macromol. Rapid Commun. **36**, 1115–1121 (2015).
[42]J. Smrek and A. Y. Grosberg, "Minimal surfaces on unconcatenated polymer rings in melt," ACS Macro Lett. **5**, 750–754 (2016).
[43]D. G. Tsalikis, V. G. Mavrantzas, and D. Vlassopoulos, "Analysis of slow modes in ring polymers: Threading of rings controls long-time relaxation," ACS Macro Lett. **5**, 755–760 (2016).
[44]D. Michieletto and M. S. Turner, "A topologically driven glass in ring polymers," Proc. Natl. Acad. Sci. U. S. A. **113**, 5195–5200 (2016).
[45]T. Ge, S. Panyukov, and M. Rubinstein, "Self-similar conformations and dynamics in entangled melts and solutions of nonconcatenated ring polymers," Macromolecules **49**(2), 708–722 (2016).
[46]D. Michieletto, N. Nahali, and A. Rosa, "Glassiness and heterogeneous dynamics in dense solutions of ring polymers," Phys. Rev. Lett. **119**, 197801 (2017).
[47]P.-G. de Gennes, "Reptation of a polymer chain in the presence of fixed obstacles," J. Chem. Phys. **55**, 572–579 (1971).
[48]M. Doi and S. F. Edwards, *The Theory of Polymer Dynamics* (Oxford University Press, New York, 1986).
[49]M. Rubinstein and R. H. Colby, *Polymer Physics* (Oxford University Press, New York, 2003).
[50]P. Chaudhuri, L. Berthier, and W. Kob, "Universal nature of particle displacements close to glass and jamming transitions," Phys. Rev. Lett. **99**, 060604 (2007).
[51]R. Metzler, J.-H. Jeon, A. G. Cherstvy, and E. Barkai, "Anomalous diffusion models and their properties: Non-stationarity, non-ergodicity, and ageing at the centenary of single particle tracking," Phys. Chem. Chem. Phys. **16**, 24128–24164 (2014).
[52]K. Kremer and G. S. Grest, "Dynamics of entangled linear polymer melts: A molecular-dynamics simulation," J. Chem. Phys. **92**, 5057–5086 (1990).

[53]R. Auhl, R. Everaers, G. S. Grest, K. Kremer, and S. J. Plimpton, "Equilibration of long chain polymer melts in computer simulations," J. Chem. Phys. **119**, 12718–12728 (2003).
[54]R. Everaers and M. R. Ejtehadi, "Interaction potentials for soft and hard ellipsoids," Phys. Rev. E **67**, 041710 (2003).
[55]S. Plimpton, "Fast parallel algorithms for short range molecular dynamics," J. Comput. Phys. **117**, 1–19 (1995).
[56]A. Rosa and R. Everaers, "Structure and dynamics of interphase chromosomes," PLoS Comput. Biol. **4**, e1000153 (2008).
[57]N. Uchida, G. S. Grest, and R. Everaers, "Viscoelasticity and primitive-path analysis of entangled polymer liquids: From F-actin to polyethilene," J. Chem. Phys. **128**, 044902 (2008).
[58]M. Pütz, K. Kremer, and G. S. Grest, "What is the entanglement length in a polymer melt?," Europhys. Lett. (EPL) **49**, 735 (2000).
[59]L. Van Hove, "Correlations in space and time and born approximation scattering in systems of interacting particles," Phys. Rev. **95**, 249–262 (1954).
[60]J.-H. Jeon, M. Javanainen, H. Martinez-Seara, R. Metzler, and I. Vattulainen, "Protein crowding in lipid bilayers gives rise to non-gaussian anomalous lateral diffusion of phospholipids and proteins," Phys. Rev. X **6**, 021006 (2016).
[61]W. Deng and E. Barkai, "Ergodic properties of fractional brownian-langevin motion," Phys. Rev. E **79**, 011112 (2009).
[62]H. S. Varol, F. Meng, B. Hosseinkhani, C. Malm, D. Bonn, M. Bonn, A. Zaccone, and S. H. Parekh, "Nanoparticle amount, and not size, determines chain alignment and nonlinear hardening in polymer nanocomposites," Proc. Natl. Acad. Sci. U. S. A. **114**, E3170–E3177 (2017).